

# An integrated modelling framework of catchment-scale ecohydrological processes: 2. The role of water subsidy by overland flow on vegetation dynamics in a semi-arid catchment

Guo-Yue Niu,<sup>1\*,†</sup> Peter A. Troch,<sup>1,2</sup> Claudio Paniconi,<sup>3</sup> Russell L. Scott,<sup>4</sup> Matej Durcik,<sup>1,5</sup>  
Xubin Zeng,<sup>1,6</sup> Travis Huxman,<sup>7</sup> David Goodrich<sup>4</sup> and Jon Pelletier<sup>1,8</sup>

<sup>1</sup> Biosphere 2 Earth Science, University of Arizona, Tucson, AZ, USA

<sup>2</sup> Department of Hydrology and Water Resources, University of Arizona, Tucson, AZ, USA

<sup>3</sup> Centre Eau Terre Environnement, Institut National de la Recherche Scientifique (INRS-ETE), Université du Québec, Québec City, Canada

<sup>4</sup> Southwest Watershed Research Center, USDA-ARS, Tucson, AZ, USA

<sup>5</sup> SAHRA (Sustainability of semi-arid hydrology and riparian areas), University of Arizona, Tucson, AZ, USA

<sup>6</sup> Department of Atmospheric Sciences, University of Arizona, Tucson, AZ, USA

<sup>7</sup> School of Biological Sciences, University of California–Irvine, Irvine, CA, USA

<sup>8</sup> Department of Geosciences, University of Arizona, Tucson, AZ, USA

## ABSTRACT

In water-limited regions, surface water and carbon fluxes are strongly controlled by soil water availability, which may be highly variable at very small spatial scales (e.g. metres) because of variations in terrain, soils, and vegetation conditions and to processes of water redistribution along hillslopes. This second of a two-part paper first evaluates the performance of a newly developed ecohydrological model over a small semi-arid experimental catchment (7.92 ha) in southeastern Arizona. Secondly, it investigates the effects of soil properties on water subsidy resulting from lateral overland flow re-infiltration and on overall ecohydrological response.

With optimized parameters, the model shows a higher ability to simulate surface energy and water fluxes than CO<sub>2</sub> fluxes at all temporal scales. The model simulates observed CO<sub>2</sub> fluxes fairly well at diurnal scales during the main growing seasons and the interannual variability of these fluxes in response to soil moisture variations from drought years to wet years. However, the model reproduces less well carbon assimilation in spring and positive CO<sub>2</sub> flux pulses following early monsoon rain events, suggesting a need for further development of the model's representations of multiple plant species and soil carbon decomposition. The model simulates soil moisture at 5 cm much better than at 15 cm mainly because of heterogeneous soil properties. Through five numerical experiments with varying saturated hydraulic conductivity values, it is revealed that the discharge at the outlet of this semi-arid catchment is essentially attributed to lateral overland flow that is generated mainly by infiltration-excess runoff. Subsurface flow plays a minor role in this semi-arid catchment with a very deep groundwater table (>100 m). The model produces wetter soils in lowland areas along stream rills and channels through re-infiltration of lateral overland flow. This water subsidy provides plants with favourable conditions to produce more leaves, CO<sub>2</sub>, and ET fluxes in lowland areas. Re-infiltration of overland flow over complex terrain may play a role in buffering climatic impacts in a warming climate with fewer but more intense rainfall events in the Southwestern United States. Copyright © 2013 John Wiley & Sons, Ltd.

KEY WORDS overland flow; re-infiltration; vegetation dynamics; semi-arid catchment

Received 14 May 2013; Accepted 30 May 2013

## INTRODUCTION

Arid and semi-arid ecosystems cover about 41% of Earth's land surface (Reynolds *et al.*, 2007) and are vulnerable to climate change. This coverage is expected to increase (Seager *et al.*, 2007) because of expansion of the Hadley cell (Lu *et al.*, 2007) and the positive vegetation-albedo

feedback to the atmospheric energy budgets (Zeng and Yoon, 2009). Zeng and Yoon (2009) projected a 34% expansion of desert areas using an Earth system model with vegetation-albedo feedback, 24% more than the Intergovernmental Panel on Climate Change Assessment Report 4 model projections that did not include this feedback. Decreases in soil moisture and vegetation cover triggered by global warming-induced drought may feed back to alter the atmospheric energy budgets and circulation through the exchanges of energy, water, and carbon fluxes between the land surface and the atmosphere (e.g. Charney, 1975; Xue and Shukla, 1993; Zeng *et al.*,

\*Correspondence to: Guo-Yue Niu, Biosphere 2 Earth Science, University of Arizona, PO Box 8746, Tucson, AZ 85738, USA.  
E-mail: niug@email.arizona.edu

†Current address: Department of Hydrology and Water Resources, University of Arizona, Tucson, AZ, USA

1999; Jin and Miller, 2007). Accurate determination of land surface energy, water, and carbon fluxes associated with changes in soil moisture and vegetation conditions over arid and semi-arid regions is thus of great importance for climate projections.

Soil water strongly controls the partitioning of available energy into sensible and latent heat fluxes and the partitioning of precipitation into evapotranspiration (ET) and runoff, two key processes that need to be properly represented in the land surface component of a climate model (Henderson-Sellers *et al.*, 2003). In arid and semi-arid regions, the ratio of runoff to precipitation becomes small, and the Horton index (defined as the ratio of ET to infiltration) becomes large (Troch *et al.*, 2009). Therefore, accurately modelling soil water can potentially improve the simulation of surface energy (sensible and latent heat), water (ET and runoff), and carbon (photosynthesis and respiration) fluxes. Soil moisture also controls ecosystem dynamics, especially in arid and semi-arid regions, where transpiration, carbon assimilation, and biomass production are limited by soil water availability during the growing season. In water-limited regions, vegetation experiences water stress, which may be highly heterogeneous at small spatial scales (e.g. metres) because of variations in terrain, soils, and vegetation conditions. Within a catchment, vegetation is organized as a signature of water availability that is generated by convergent flow networks (Caylor *et al.*, 2004; Thompson *et al.*, 2011). On the other hand, spatially distributed vegetation exerts a feedback to ET distributions and the catchment water balance (e.g. Emanuel *et al.*, 2010; Thompson *et al.*, 2011). Both lateral water flows of surface water and subsurface water along flow networks in a catchment contribute to water availability in convergent zones. Spatially distributed, physically based numerical models may facilitate understanding of the relative roles of surface and subsurface flows in controlling water availability and ecohydrological response.

Early land surface models (LSMs) (Sellers *et al.*, 1986; Dickinson *et al.*, 1993) designed for climate studies did not explicitly consider soil moisture variations induced by subgrid variations in topography, soil properties, and vegetation type. Later, LSMs represented the effects of subgrid variations in soil moisture on surface fluxes using a steady-state assumption but neglected the effects of transient lateral water flow (Entekhabi and Eagleson, 1989; Liang *et al.*, 1994; Famiglietti and Wood, 1994; Koster *et al.*, 2000; Niu *et al.*, 2005). In the most recent developments, LSMs have been coupled with three-dimensional (3D) hydrological models (Fan *et al.*, 2007; Maxwell and Kollet, 2008; Kollet and Maxwell, 2008; Pan *et al.*, 2008; Niu *et al.*, 2013) to resolve the interactions between hydrological, ecological, and atmospheric processes at a higher spatial resolution. Some of these

studies have shown that lateral flow of groundwater can have a significant effect on soil moisture and thus on surface energy and water fluxes (Miguez-Macho *et al.*, 2008; Maxwell and Kollet, 2008; Kollet, 2009).

In arid or semi-arid regions, groundwater may be too deep to have an effect on soil moisture and surface water and energy fluxes. However, rainfall may be efficiently redistributed over complex terrain through lateral overland flow. The role of overland flow in regard to ecohydrological dynamics has not been addressed in previous studies. In this paper, we try to answer the following questions: (1) How do soil properties (e.g. saturated hydraulic conductivity) affect infiltration and thus generation of overland water flows and surface flux exchanges with the atmosphere? and (2) how and to what extent does lateral overland flow affect soil water availability and water and carbon flux exchanges with the atmosphere? We first evaluate the newly developed 3D, physically based, spatially distributed CATHY/NoahMP ecohydrological model described in part 1 of this two-part paper (Niu *et al.*, 2013) against observational data from a well-instrumented experimental watershed in Southwestern United States. We then design sensitivity experiments by altering the saturated hydraulic conductivities ( $K_s$ ) in both horizontal and vertical directions to investigate the effects of this key soil parameter on production of overland flow and water redistribution over the catchment and to examine the impacts of this water subsidy on ecohydrological response.

## EXPERIMENTAL WATERSHED AND DATA

The Kendall grassland watershed (31.74° N, 109.94° W, 1515–1540 m) is located in the upper end of the US Department of Agriculture (USDA) Agricultural Research Service (ARS) Walnut Gulch Experimental Watershed (Moran *et al.*, 2008; Scott *et al.*, 2010). The land surface is covered mainly by C4 bunchgrasses during the study period (2004–2009) with changes from native bunchgrasses (2003–2006) to the exotic C4 Lehmann lovegrass (2007–2009) due to drought-induced mortality of the native species (Scott *et al.*, 2010). The soils are generally sandy to fine-sandy loams with some areas having silty-clay to clay loams. The annual mean rainfall is 345 mm, of which 63% comes from the summer monsoon, and the mean annual temperature is 17.4 °C. Depth to groundwater is on the order of 100 m (Spangler, 1969). Figure 1 shows the 4 m resolution digital elevation model of the 7.92 ha catchment measured with Laser Imaging Detection and Ranging (LIDAR) and the upstream area,  $a$ , derived with the pre-processor of CATHY scaled by the natural logarithm, i.e.  $\ln(a)$ , which clearly shows stream channels. An eddy covariance flux tower is located at the southeastern upstream corner of the catchment. The tower has a flux footprint that depends on wind direction and

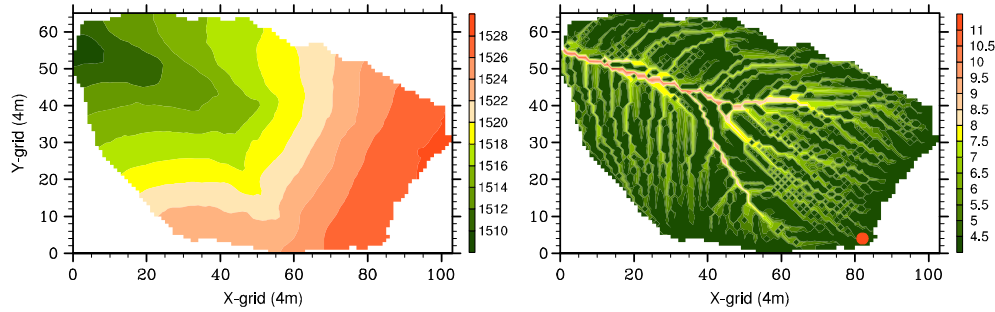


Figure 1. The digital elevation model (left); meter and the upstream area,  $a$ , scaled by natural logarithm,  $\ln(a)$  (right), of the Kendall catchment at 4 m resolution. The location of the flux tower is also shown (red dot in right map).

atmospheric turbulence characteristics and sometimes extends beyond the catchment boundaries, which may result in observed fluxes that deviate from modelled catchment average fluxes.

The observational dataset at the site is available publicly for ‘fair-use’ (<ftp://cdiac.ornl.gov/pub/ameriflux>). It includes half-hourly near-surface micrometeorological data of incoming shortwave radiation, downward longwave radiation, 3 m air temperature and humidity, 6 m CO<sub>2</sub> concentrations and wind speed, air pressure, and precipitation for driving the model. It also includes fluxes of net radiation, outgoing longwave radiation, sensible heat, latent heat, ground heat, CO<sub>2</sub> [or net ecosystem exchange (NEE)], and runoff as well as state variables of soil moisture and temperature for evaluating the model. The wind speed at 6 m,  $U_{6m}$  [m s<sup>-1</sup>], was interpolated to 3 m using a log-linear wind profile:  $U_{3m} = U_{6m} \ln(3/z_0) / \ln(6/z_0)$ , where  $z_0$  (m) is the surface roughness length. Most of the observational forcing data have a missing data occurrence of less than 1%, except for the incoming longwave radiation that has 21.4%, 3.5%, and 18.9% missing data for 2005, 2007, and 2008, respectively. The CATHY/NoahMP model requires continuous near-surface micrometeorological forcing data, so we estimated the incoming longwave radiation as a function of atmospheric temperature and humidity following Idso (1981) for clear sky without consideration of cloud effects:

$$L_{\downarrow} = \left( C_1 + C_2 e_a e^{\frac{1500}{T_a}} \right) \sigma T_a^4 \quad (1)$$

where  $\sigma$  is the Stefan–Boltzmann constant ( $=5.67 \times 10^{-8}$  W m<sup>-2</sup> K<sup>-4</sup>);  $T_a$  and  $e_a$  are atmospheric temperature (K) and water vapour pressure (Pa), respectively; and  $C_1$  and  $C_2$  are empirical parameters. We changed  $C_1$  and  $C_2$  from their default values (0.70 and  $5.95 \times 10^{-7}$ ) to 5.5 and  $1.2 \times 10^{-6}$ , respectively, to match the observed data when they were available.

### MODEL EXPERIMENTS

We conducted five pairs of experiments by varying  $K_s$  values in either horizontal or vertical directions with each pair having two experiments without and with mass imbalance corrections (Table II). The control experiment (CTRL) was calibrated against the total amount of observed ET, discharge, and NEE (or net CO<sub>2</sub> fluxes) for the entire modelling period and the half-hourly energy and CO<sub>2</sub> fluxes observed during the growing season of 2007 (Figure 2). The resulting  $K_s$  value for both vertical and lateral directions is  $1.25 \times 10^{-7}$  m s<sup>-1</sup>. Experiments L1 and L2 were conducted by changing the lateral  $K_s$  value to a smaller value of  $1.25 \times 10^{-9}$  m s<sup>-1</sup> (L1) to shut off lateral subsurface flow and to a greater value of  $1.25 \times 10^{-4}$  m s<sup>-1</sup> (L2) to increase lateral subsurface flow. Experiments V1 and V2 were conducted by changing the vertical  $K_s$  value to a smaller value of  $1.25 \times 10^{-8}$  m s<sup>-1</sup> (V1) to decrease the infiltration rate and to a greater value of  $1.25 \times 10^{-6}$  m s<sup>-1</sup> (L2) to increase infiltration and thus reduce overland flow and discharge. For the unsaturated soil hydraulic characteristics, a van Genuchten and Nielsen (1985) fitting parameter  $n = 2.5$  was used.

The five experiments with corrections to mass imbalance first compute the residual ( $ERR$ ) of the water budgets:  $ERR = q_{in} - q_{root} - q_{dis} - \Delta S$ , where  $q_{in}$ ,  $q_{root}$ , and  $q_{dis}$  are water fluxes incident on the soil surface (including drip from the vegetation canopy-intercepted water, throughfall, snowmelt, and surface dew or evaporation; Niu *et al.*, 2013), transpiration through root uptake, and discharge at the outlet, respectively; and  $\Delta S$  is the change in total water storage including water stored in subsurface soil and surface ponds.  $ERR$  is then distributed to unsaturated elements in proportion to the water content of these elements to update their volumetric water content, which is, in turn, converted to pressure according to the water retention relationship of van Genuchten and Nielsen (1985).

We ran the five pairs of experiments at a constant time step of 1800 s for NoahMP and at timesteps varying from 0.1 to 900 s for CATHY (see Niu *et al.*, 2013 for details on

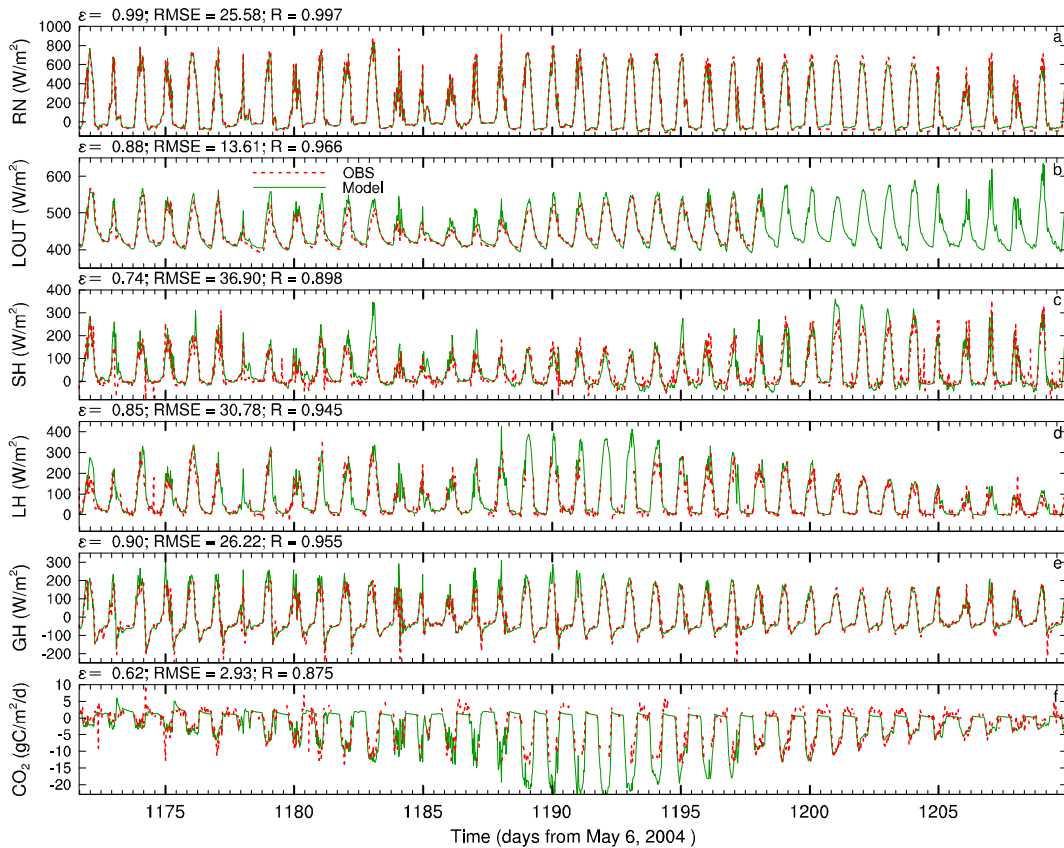


Figure 2. Comparison of observed (OBS) and modelled (Model) half-hourly fluxes of net radiation (a), outgoing longwave radiation (b), sensible heat (c), latent heat (d), ground heat (e), and  $\text{CO}_2$  (f) during the growing season of 2007 at the Kendall subwatershed of Walnut Gulch, Arizona. On the top of each panel, model efficiency ( $\epsilon$ ), root mean squared error (RMSE), and correlation coefficient ( $R$ ) are listed for each variable.

the time stepping procedures used in the coupled version of the ecohydrological model). We conducted two successive spin-up runs from 6 May 2004 to the end of 2009 (>11 years) to obtain initial conditions of subsurface soil water pressure, temperature, and carbon storage for each of the 10 experiments.

All five pairs of experiments used the same model setup as well as soil and vegetation parameters except for  $K_s$  values. The coupled model was set up with four soil layers: 0–0–0.1, 0.1–0.4, 0.4–1.0, and 1.0–2.0 m. The side and bottom (2.0 m deep) boundaries are sealed with zero-flux boundary conditions. A zero-flux bottom boundary condition is considered appropriate because groundwater recharge during the rainy season is low because of the typical short duration of rainfall events and rapid post-storm drying (Goodrich *et al.*, 2004). We selected sandy loam as the soil type for this site out of the 19 soil types represented by NoahMP. The NoahMP default and calibrated soil parameters are listed in Table I. In this semi-arid region, calibration of the soil parameters that control water stress is critical for the modelling results of vegetation dynamics and  $\text{CO}_2$  assimilation. Calibration of the wilting point and reference soil moisture (which

determine the water stress factor defined as the relationship between soil moisture and transpiration) to smaller values increases the plants' water use efficiency. The soil colour index controls surface albedo at this sparsely vegetated site; it is calibrated to 5 against the observed net radiation at midday hours (1 represents lightest and 8 represents darkest soil colour).

The model resolves vegetation at a level of type and not of species. We selected C4 warm grass as the vegetation type without representing the evolution from bunchgrass to Lehmann lovegrass that occurred during the study period (Scott *et al.*, 2010). We calibrated three major vegetation parameters against the Moderate-resolution Imaging Spectroradiometer (MODIS) derived leaf area index (LAI) and observed net  $\text{CO}_2$  fluxes. Calibration of the optimum carboxylation rate at 298 K from 40 to 110  $\mu\text{mol m}^{-2} \text{s}^{-1}$  greatly increases carbon assimilation and leaf area. Because of this change, other parameters such as specific leaf area and leaf dying rate due to drought have to be adjusted to decrease the leaf area in order to match the MODIS-derived LAI. The specific leaf area was calibrated from 60  $\text{m}^2 \text{kg}^{-1}$  (a value calibrated against MODIS LAI over North America; see Niu *et al.*, 2011) to 12  $\text{m}^2$

Table I. Soil and vegetation parameters.

	Parameters	Default	Calibrated
Soil	Soil porosity ( $\text{m}^3 \text{m}^{-3}$ )	0.434	0.45
	Wilting point ( $\text{m}^3 \text{m}^{-3}$ )	0.047	0.032
	van Genuchten $n$	—	2.5
	Saturated matrix potential (m)	-0.141	-0.45
	Reference soil moisture ( $\text{m}^3 \text{m}^{-3}$ )	0.383	0.360
	Soil colour index (1 → lightest ; 8 → darkest)	—	5
Vegetation	Specific leaf area ( $\text{m}^2 \text{kg}^{-1}$ )	60	12
	Optimum carboxylation rate ( $\mu\text{mol m}^{-2} \text{s}^{-1}$ )	40	110
	Root depth (m)	1.0	0.4
	Leaf dying rate due to drought ( $1 \times 10^{-6} \text{s}^{-1}$ )	0.20	0.60

$\text{kg}^{-1}$ , whereas the leaf dying rate due to drought was tripled. The roots were evenly distributed, and the root-zone depth was calibrated to 0.4 m from its default value of 1.0 m. This change makes the plants more responsive. NoahMP has three options for the water stress factor. We selected, for all the experiments, the Noah-type factor, which has a lower wilting point and a smaller slope against soil moisture than the other options (Niu *et al.*, 2011).

All the model experiments were conducted at a horizontal grid resolution of 4 m. It should be noted that, consistent with such high-resolution, process-based hydrological modelling, high-resolution atmospheric turbulence modelling (e.g. large eddy simulation) could be considered. However, in this study, we use atmospheric variables measured at a few metres (e.g. 3 m for air temperature and humidity) over short plants (i.e. grass). It is reasonable to assume that the eddies between the ground roughness length ( $\sim 0.05$  m) and a few metres above ground are homogeneous and isotropic, ensuring validity of the Monin–Obukhov similarity theory to parameterize the turbulent exchanges of energy and mass between the land surface and the atmosphere. As such, the atmospheric forcing data measured at the local site are applied at each cell over the entire catchment. This procedure can be justified by the fact that horizontal heterogeneity of atmosphere variables is much weaker than that of soil water and plants because of the more efficient mixing of air through eddies in the surface layer (relative to diffusion of water and heat in the subsurface soil).

## RESULTS

### Mass balance analyses

We first analysed the mass balance resulting from the five pairs of experiments. Without corrections, the five experiments with various  $K_s$  produced very different *ERR* values, which are negative for smaller  $K_s$  values (CTRL, L1, and V1) and positive for larger  $K_s$  values (L2 and V2)

(Table II). V1, which has the smallest vertical  $K_s$ , results in the most significant *ERR* ( $-194$  mm), whereas CTRL produces the smallest ( $-28$  mm). Comparing each experiment without corrections with that with corrections for the five pairs, we find that corrections to *ERR*, i.e. the amount of water that is put back to the soil, have the greatest impact on *ET*, while affecting runoff (*R*) the least. For instance, V1, the most serious case, produces  $-194$  mm *ERR* during the entire modelling period, of which  $-200$  mm is distributed to *ET* and 7 mm to *DS*, the residual water stored in the soil at the end of the simulation. For all cases, the corrections to runoff are less than 1 mm, which is relatively small compared with the total amount of modelled runoff. With the calibrated soil and vegetation parameters, CTRL produces total amounts of *ET* (1368 mm) and *R* (92 mm) that are comparable with but slightly smaller than the observed values (1399 and 98 mm for *ET* and runoff, respectively), because of the 38 mm of *DS*. For smaller  $K_s$  values, *DS* values are positive (CTRL, L1, and V1), whereas *DS* is  $\sim 0$  mm for greater  $K_s$  values (L2 and V2). This indicates that the model needs a longer spin-up time to reach an equilibrium state for small  $K_s$  values. The optimized  $K_s$  from calibration (CTRL) is unexpectedly small ( $1.25 \times 10^{-7} \text{m s}^{-1}$ ), most probably because the half-hourly rainfall rate is not large enough to generate infiltration-excess overland flow. The rainfall rate becomes artificially small when storms occurring over a very short period are averaged over the half-hour model time step.

### Model evaluation

#### Surface energy, water, and $\text{CO}_2$ fluxes at diurnal scales.

The observed energy fluxes are not balanced. We first computed the residual of the observed energy budgets ( $R_n - H - LE - G$ , where  $R_n$ ,  $H$ ,  $LE$ , and  $G$  are net radiation, sensible heat, latent heat, and ground heat fluxes) and then distributed it to  $H$ ,  $LE$ , and  $G$  in proportion to their ratios to  $R_n$ , respectively, to balance the surface energy budgets. The modelled half-hourly, catchment-averaged

Table II. Model experiments and results.

	CTRL		L1		L2		V1		V2		OBS
	No	Yes									
$K_{sat}$											
<i>x</i>	$1.25 \times 10^{-7}$		$1.25 \times 10^{-9}$		$1.25 \times 10^{-4}$		$1.25 \times 10^{-7}$		$1.25 \times 10^{-7}$		$1.25 \times 10^{-7}$
<i>y</i>	$1.25 \times 10^{-7}$		$1.25 \times 10^{-9}$		$1.25 \times 10^{-4}$		$1.25 \times 10^{-7}$		$1.25 \times 10^{-7}$		$1.25 \times 10^{-7}$
<i>z</i>	$1.25 \times 10^{-7}$		$1.25 \times 10^{-7}$		$1.25 \times 10^{-7}$		$1.25 \times 10^{-8}$		$1.25 \times 10^{-6}$		$1.25 \times 10^{-6}$
<i>P</i>	1499		1499		1499		1499		1499		1499
Correction	No	Yes									
<i>ET</i>	1405	1369	1405	1369	1436	1478	1422	1222	1400	1500	1399
<i>R</i>	93	92	91	91	20	20	242	241	0	0	98
<i>DS</i>	29	38	43	39	-4	0	29	36	-5	-1	2
<i>ERR</i>	-28	0	-39	0	46	0	-194	0	103	0	
$E_{soil}$	1030	970	1031	971	1075	1059	1102	922	1115	1138	
$E_{can}$	16	16	16	16	15	16	15	14	13	14	
$E_{ren}$	359	383	358	382	346	404	305	286	273	347	
<i>NEE</i>	-0.25	-0.25	-0.25	-0.25	-0.23	-0.27	-0.21	-0.17	-0.16	-0.22	-0.27

Model experiments (CTRL, L1, L2, V1, and V2) with values of saturated hydraulic conductivity ( $K_s$ ;  $m s^{-1}$ ); modelled water budget components including precipitation ( $P$ ; mm), evapotranspiration ( $ET$ ; mm), runoff ( $R$ ; mm), total water storage change ( $DS$ ; mm), and residual ( $ERR$ ; mm);  $ET$  components including evaporation from soil surface ( $E_{soil}$ ; mm), interception loss ( $E_{can}$ ; mm), and transpiration ( $E_{ren}$ ; mm); and net ecosystem exchange ( $NEE$ ;  $gC m^{-2}/day$ ) resulting from pairs of experiments without (no) and with (yes) corrections to water mass imbalance.

fluxes of net radiation, outgoing longwave radiation, sensible heat, latent heat, ground heat, and  $CO_2$  fluxes produced by CTRL agree considerably well with the observed data as indicated from the model efficiencies ( $\epsilon$ ) or Nash criteria (Nash and Sutcliffe, 1970) (Figure 2).  $\epsilon$  measures a model's skill at capturing observed variability. A value of one indicates a perfect simulation, zero means that the model is capable of representing the observed temporal mean, and a negative value indicates a poor simulation. The model shows a relatively high capability of simulating net radiation, outgoing longwave, latent heat, and ground heat fluxes with  $\epsilon$  being above 0.85, whereas it is lower for sensible heat and net  $CO_2$  fluxes (0.74 and 0.62, respectively). During the dry-down period from the peak growing season (day 1195 to 1205), the model shows a capability of reproducing latent heat and  $CO_2$  fluxes, which are very sensitive to soil water availability and rooting depth, thereby suggesting the model's capability of simulating soil water during this dry-down period. The relatively low modelling skill at modelling  $CO_2$  fluxes can be mainly attributed to the mismatch for the positive segments, suggesting a further need to develop representations of respiration processes of the ecosystem.

The model shows a high skill at reproducing the diurnal cycle of the energy fluxes with  $\epsilon$  values being above 0.90 for all seasons (Figure 3). It also simulates well the diurnal variation of  $CO_2$  fluxes for major growing seasons (summer and fall). However, it shows a relatively low skill for other seasons, especially spring, resulting in a negative  $\epsilon$  value (-0.49). The model deficiency in spring may be attributed to the model's representation of a single species of C4 warm grass. A 'mosaic' representation of multiple species of C3 and C4 may improve the simulation for all seasons.

*State and fluxes at seasonal scales.* At seasonal and interannual scales, the modelled LAI, runoff, and soil moisture are comparable with the observations (Figure 4). The modelled total runoff during the entire period is 92 mm, about 6% less than the observed value (98 mm). As mentioned before, this may result from an insufficiently long spin-up run of the model, which results in a net increase in soil water storage (38 mm). Thus, longer spin-up runs would help improve the simulation but would increase the soil carbon storage and thus degrade the simulation of  $CO_2$  fluxes. As will be shown later, runoff in this arid catchment is mainly produced by infiltration excess, so further calibration of vertical  $K_s$  would also improve the simulation. The model reproduces the weekly MODIS-derived LAI for the three wet years (2006–2008). However, with the same optimized vegetation parameters, the modelled LAI is lower than the MODIS-derived LAI during the drought years (2004, 2005, and 2009), suggesting that the model should take into consideration changes in plant species and multiple species at a time. The

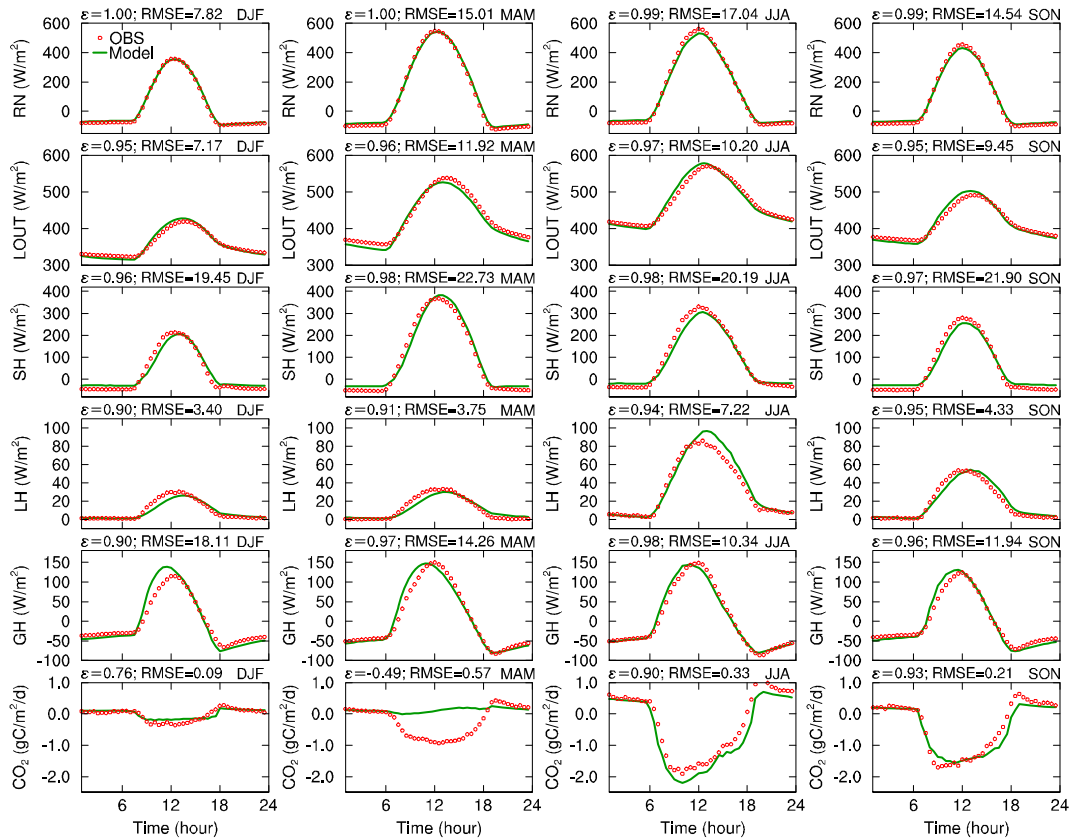


Figure 3. Comparison of observed (OBS) and modelled (by CTRL) diurnal variations in fluxes of net radiation (RN), outgoing longwave radiation (LOUT), sensible heat (SH), latent heat (LH), ground heat (GH), and  $\text{CO}_2$  averaged over all winters (DJF; December, January, and February), springs (MAM; March, April, and May), summers (JJA; June, July, and August), and falls (SON; September, October, and November) of the entire modelling period (from 6 May 2004 to the end of 2009) at the Kendall subwatershed of Walnut Gulch, Arizona.

modelled 5 cm soil moisture agrees well with the observation data but with greater-than-observed peaks during major monsoon rainfalls, most apparent during the 2006 monsoon season, which result in greater assimilation of  $\text{CO}_2$  (Figure 5f) and LAI (Figure 4a). The model captured well the variability of the observed 15 cm soil moisture (correlation coefficient is 0.87) but with a systematically low bias ( $0.03 \text{ m}^3 \text{ m}^{-3}$ ). This may be mainly attributed to higher clay content in deeper soils observed at the site. Another possible reason is that the initial conditions resulting from the 11-year spin-up run are drier than the observations.

The modelled, catchment-averaged fluxes of net radiation, outgoing longwave radiation, sensible heat, latent heat, ground heat, and  $\text{CO}_2$  from CTRL agree fairly well with the observed values (Figure 5). The largest error in the modelled net radiation occurs when the incoming longwave radiation is missing. Similarly, the disagreement for sensible heat flux increases during these same periods. Because in these dry periods the Bowen ratio is high, most of the erroneous net radiation is allocated to sensible heat flux. The modelled latent heat flux accurately captures the observed peaks and interannual variations in response to

monsoon precipitation but misses some high-frequency peaks during dry seasons.

The model simulates energy fluxes much better than  $\text{CO}_2$  fluxes. The model performs well in simulating the interannual variability of  $\text{CO}_2$  fluxes, i.e. greater negative peaks in the wet years of 2006, 2007, and 2008 and smaller negative peaks in the drought years of 2004, 2005, and 2009. However, the model's efficiency is as low as  $-0.24$ , indicating a low ability to model  $\text{CO}_2$  fluxes at seasonal scales. First, the model shows a lower-than-observed ecosystem productivity (smaller negative values) during drought years (2004, 2005, and 2009) and larger productivity in wet years (2006, 2007, and 2008). This is most likely induced by the water stress factor that may exert a too-strong water stress in the drought years and by the wilting point used in the water stress factors that may be too high. As mentioned earlier, the model should also represent multiple plant species to improve the simulation of ecosystem productivity in spring. Secondly, the model misses rapid, positive  $\text{CO}_2$  pulses following early monsoon rain events. These pulses may be induced by  $\text{CO}_2$  diffusive transport and decomposition of soil carbon accumulated during dry periods (Riveros-Iregui *et al.*, 2007; Barron-

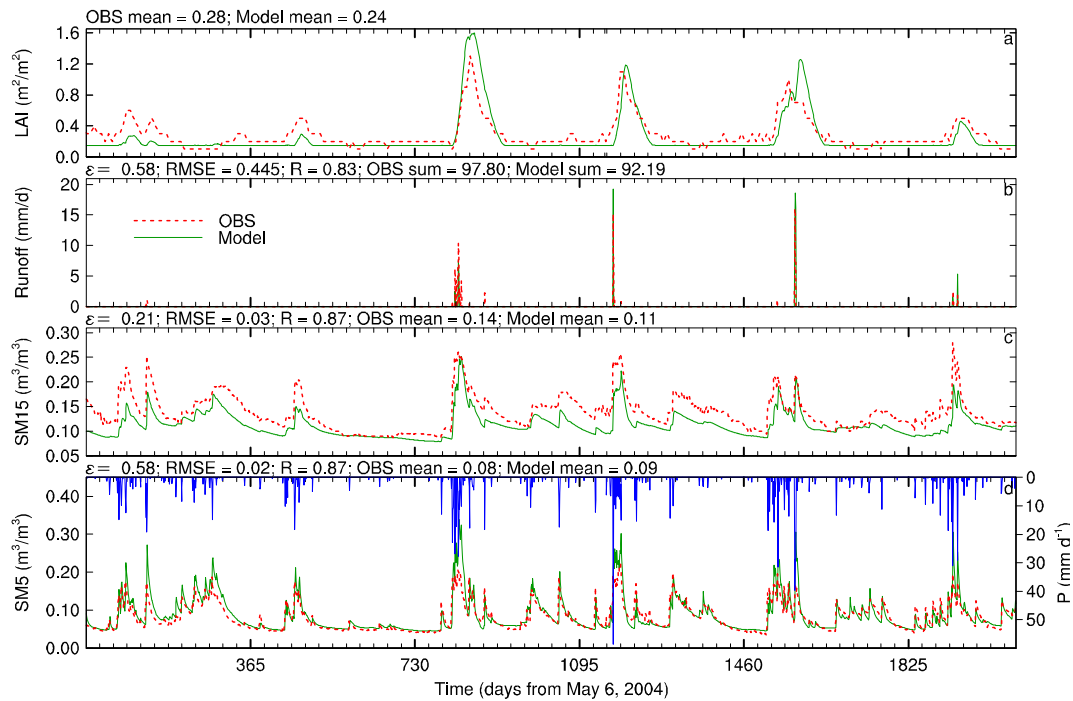


Figure 4. Modelled daily mean LAI (a), runoff (b), soil moisture at 15 cm (c), and soil moisture at 5 cm (d) by CTRL compared with observed weekly mean MODIS LAI, daily mean runoff, and soil moisture. The observed precipitation is shown in the bottom panel.

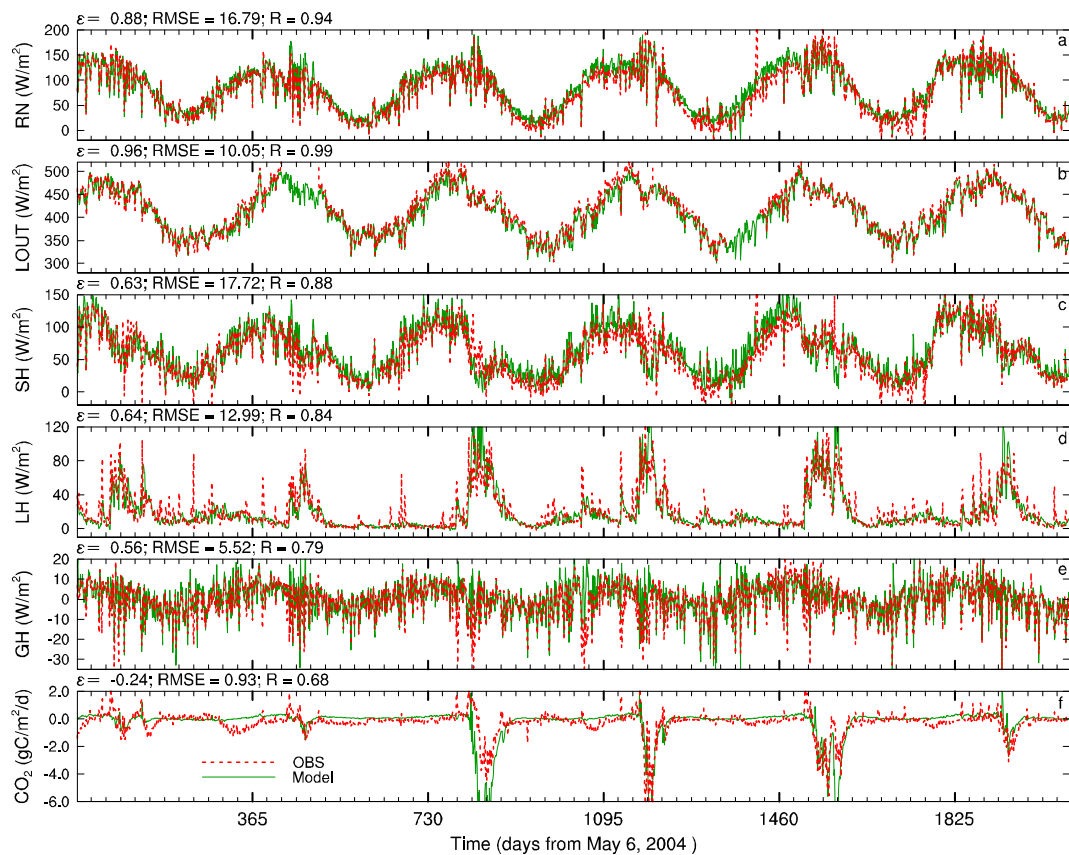


Figure 5. Comparison of observed and modelled (by CTRL) daily mean fluxes of net radiation (a), outgoing longwave radiation (b), sensible heat (c), latent heat (d), ground heat (e), and CO<sub>2</sub> (f) over the entire modelling period (6 May 2004 to end of 2009) at the Kendall subwatershed of Walnut Gulch, Arizona.

Gafford *et al.*, 2011). To improve the simulation, the model should explicitly represent more complex processes including microbial activities that are very responsive to moisture and temperature changes (Allison *et al.*, 2010; Todd-Brown *et al.*, 2012). Because of lack of understanding of these critical processes, most other ecosystem models also show a low ability to simulate CO<sub>2</sub> fluxes and ecosystem productivity as well as their interannual variability, as indicated from recent model intercomparison projects (Schwalm *et al.*, 2010; Schaefer *et al.*, 2012).

#### Effects of lateral overland flow

Figure 6 shows the comparison between CTRL, L1, and L2. L1 with the lowest lateral  $K_s$  value ( $1.25 \times 10^{-9} \text{ m s}^{-1}$ ), which was designed to shut off lateral subsurface flow, produces almost the same runoff, ET, NEE, and transpiration fluxes as CTRL. L2 with the highest lateral  $K_s$  value ( $1.25 \times 10^{-4} \text{ m s}^{-1}$ ) produces much less discharge (20 mm) and more ET (1478 mm) than CTRL (92 and 1369 mm for runoff and ET, respectively). L2 also produced slightly more plant and transpiration fluxes than CTRL mainly because of more water that is retained in the catchment.

Figure 7 shows the comparison between CTRL, V1, and V2. V1 with the smallest vertical  $K_s$  value ( $1.25 \times 10^{-8} \text{ m s}^{-1}$ ) produces the largest discharge and the least ET, whereas V2 with the largest vertical  $K_s$  value ( $1.25 \times 10^{-6} \text{ m s}^{-1}$ ) produces the least discharge and the largest ET to close the water budget. CTRL is in between. However, there is no such pattern for CO<sub>2</sub> and transpiration fluxes. CTRL results in the greatest NEE and transpiration, whereas V1 produces the least. V2 with the highest infiltration, which is expected to produce the most plant growth, results in smaller NEE ( $-443 \text{ gC m}^{-2}$ ) and

transpiration (347 mm) than CTRL ( $-508 \text{ gC m}^{-2}$  and 383 mm, respectively). In addition, V2 produces a smaller ratio of transpiration to ET (0.23) than CTRL (0.28), indicating that most of the water retained in the catchment, which is more evenly distributed in the case of V2, is evaporated from bare soil surface. However, re-infiltration of overland flow in the case of CTRL plays an important role in ecosystem productivity.

The coupled model computes lateral flow of subsurface water and explicitly computes overland flow and its re-infiltration. In the case of CTRL, the spatial distribution of LAI averaged over the entire modelling period (Figure 8) shows lower LAI values in most upland areas and higher values in the lowland areas along stream channels in response to the wetter soil. Correspondingly, the modelled ET and CO<sub>2</sub> fluxes are greater in these lowland areas. Thus, the wetter soil along stream channels can be regarded as a buffer for vegetation growth and carbon assimilation. Lateral overland flow or lateral subsurface flow or both can induce wetter soil in lowland areas. L1 effectively shuts off lateral subsurface flow and forces lateral redistribution of water to be induced by overland flow alone. Although it has a higher  $K_s$  value than L1, CTRL produced almost the same ET and transpiration fluxes as L1 (Figure 6), suggesting that CTRL also effectively shuts off lateral subsurface flow and that the spatial pattern in soil water and plants is induced by re-infiltration of overland flow. The difference between infiltration rate and precipitation rate,  $\Delta Q$  (lower two panels of Figure 8), indicates the contribution of overland flow to infiltration and in effect provides a spatial map of re-infiltration patterns. High  $\Delta Q$  areas are distributed along the stream channels and exhibit a similar pattern to soil moisture, LAI, ET, and CO<sub>2</sub> fluxes.

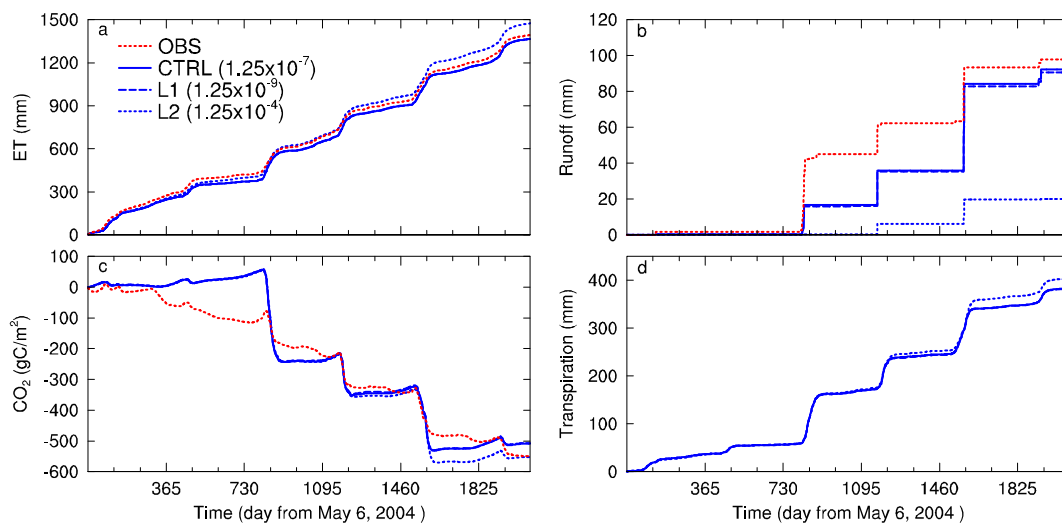


Figure 6. Cumulative ET (a), runoff (b), CO<sub>2</sub> (c), and transpiration (d) fluxes resulting from the experiments with varying lateral  $K_s$  (CTRL, L1, and L2) at the Kendall watershed of Walnut Gulch, Arizona.

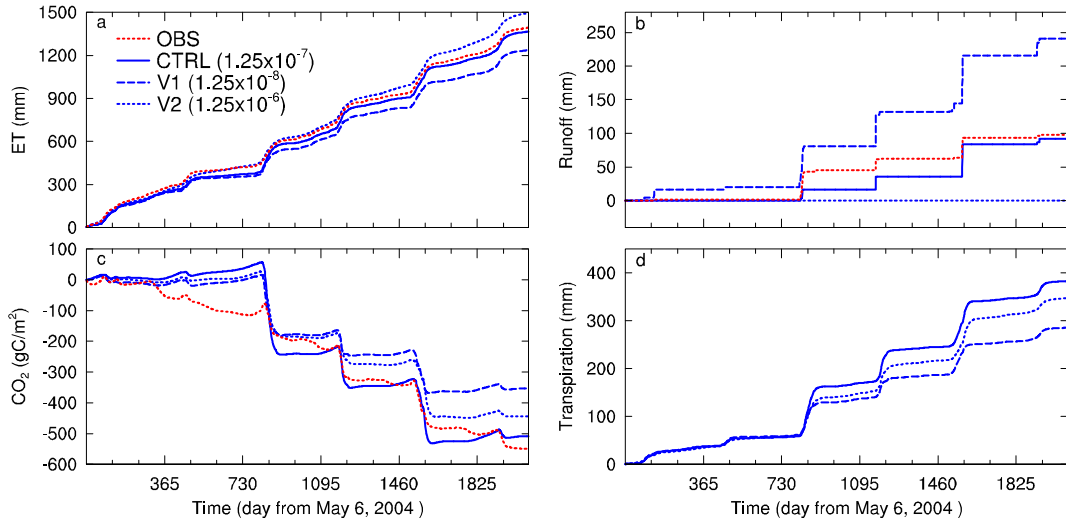


Figure 7. Cumulative ET (a), runoff (b), CO<sub>2</sub> flux (c), and transpiration (d) fluxes resulting from the experiments with varying vertical  $K_s$  (CTRL, V1, and V2) at the Kendall subwatershed of Walnut Gulch, Arizona.

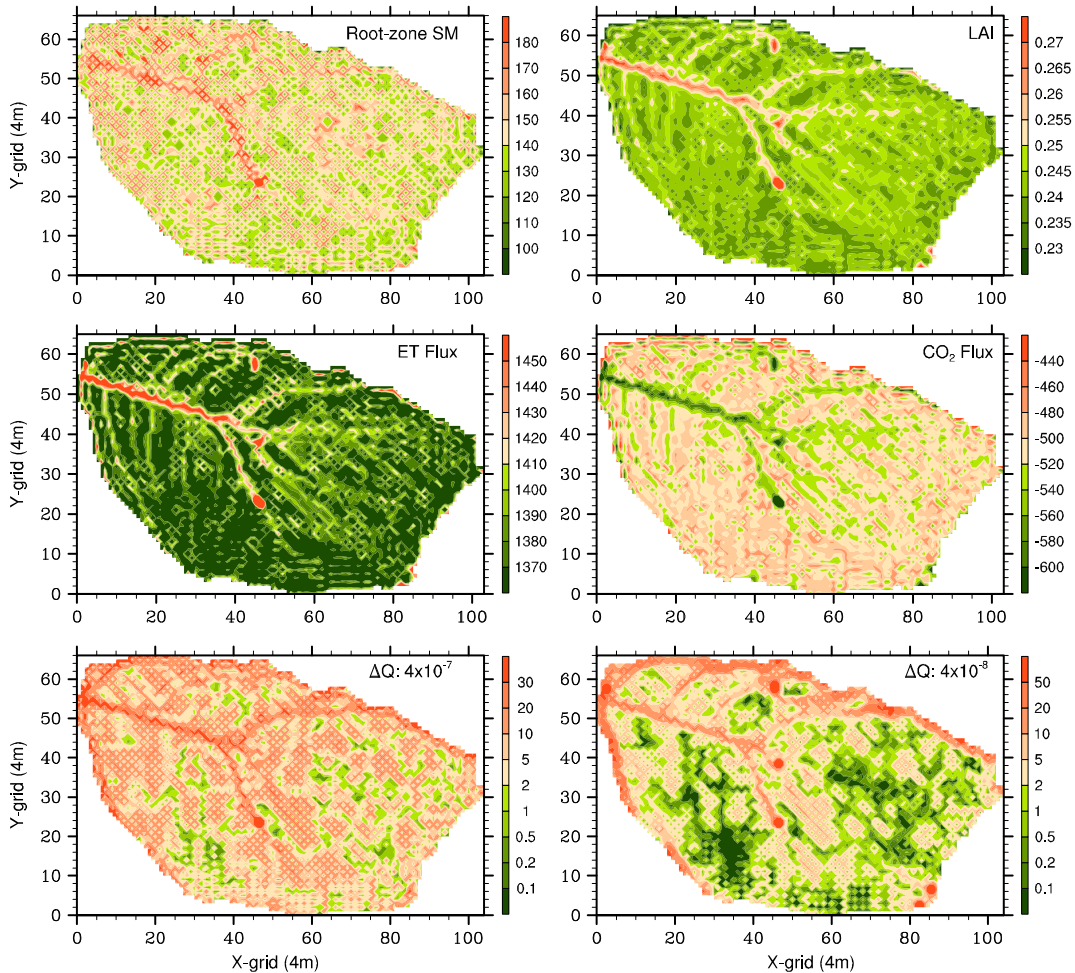


Figure 8. Spatial distribution of averaged root-zone soil moisture (mm) and LAI (upper two panels) and cumulative ET fluxes (mm day<sup>-1</sup>) and CO<sub>2</sub> fluxes (gC m<sup>-2</sup>) over the entire modelling period. The lower two panels show re-infiltration maps, i.e. the difference between infiltration rate and precipitation rate ( $\Delta Q$ ; mm) accumulated over the entire modelling period for CTRL (left) and V1 (right) experiments.

The wetter soil at a given computational cell in lowland areas is mainly attributed to re-infiltration of additional water inputs from lateral overland flow originating from upslope computational cells. As expected, CTRL-produced  $\Delta Q$  is less pronounced along the stream channels and more uniformly distributed over the catchment compared with V1, because of more direct infiltration for CTRL and thus less lateral overland flow and re-infiltration. An additional consequence of this, seen in Figure 7b, is that CTRL-produced discharge at the outlet of the catchment is smaller than that of V1.

The resulting runoff from experiments CTRL, V1, and V2 reflects the runoff generation mechanism in this semi-arid catchment (Figures 6b and 7b). CTRL ( $K_s = 1.25 \times 10^{-7} \text{ m s}^{-1}$ ) produced 92 mm runoff for the entire modelling period, close to the observed 98 mm. V1 with the smaller vertical  $K_s$  ( $1.25 \times 10^{-8} \text{ m s}^{-1}$ ) produced too much runoff (241 mm), whereas V2 with the greater vertical  $K_s$  ( $1.25 \times 10^{-6} \text{ m s}^{-1}$ ) does not produce any runoff at all. With a small vertical  $K_s$ , the precipitation rate can readily exceed the infiltration rate, and the excessive water over each 4 m grid cell then flows along rills and channels to the outlet of the catchment, with part of the water re-infiltrating into soils along rills and channels. A larger vertical  $K_s$  facilitates infiltration of surface water into deeper soils and aquifers under gravity, rather than flowing laterally. In this semi-arid catchment, overland flow generated by the infiltration-excess (Hortonian) mechanism can be regarded as an additional driver for plant growth, and re-infiltration of overland flow over complex terrain may play a role in buffering climatic impacts in a warming climate with less but more intense rainfall in the Southwestern United States.

## SUMMARY

In this study, we first evaluated the performance of the newly developed 3D, physically based, spatially distributed CATHY/NoahMP ecohydrological model over a small semi-arid experimental catchment (7.92 ha) in southeastern Arizona. Secondly, we investigated the effects of saturated hydraulic conductivity on water subsidy resulting from lateral overland flow re-infiltration and on ecohydrological response.

We conducted five pairs of experiments with and without mass corrections by varying  $K_s$  values in both lateral and vertical directions. Over this water-limited catchment, the mass imbalance from the experiments without corrections is not negligible compared with other water budget terms (e.g. runoff and transpiration), especially for the two experiments (V1 and V2) for which the vertical  $K_s$  values were varied. The mass correction scheme, which returns the residual water computed from

the water balance equation to the soil to correct soil moisture and pressure, effectively eliminated the imbalance of mass produced by the model. As a result of the correction, the water imbalance is mainly allocated to ET and proportionally to its other components, with a very small effect on runoff in this water-limited catchment, which is mainly generated by infiltration-excess overland flow.

With optimized parameters, the model shows a higher ability to simulate surface energy and water fluxes than  $\text{CO}_2$  fluxes at all temporal scales. The model simulates fairly well  $\text{CO}_2$  fluxes at diurnal scales during the main growing season and  $\text{CO}_2$  flux interannual variability in response to soil moisture variations from drought years to wet years. However, the model shows a low ability of simulating negative  $\text{CO}_2$  flux in spring, and it fails to simulate positive  $\text{CO}_2$  flux pulses following early monsoon rain events, suggesting a need for further development to represent multiple plant species (or types) and soil carbon decomposition. The model simulates soil moisture at 5 cm much better than that at 15 cm mainly because of heterogeneous soil properties. Through five numerical experiments with varying saturated hydraulic conductivity values, it is revealed that the discharge at the outlet of this semi-arid catchment is essentially attributed to lateral overland flow that is generated mainly by infiltration-excess (Hortonian) runoff. Subsurface flow plays a minor role in this semi-arid catchment with a very deep groundwater table (>100 m) (Spangler, 1969). The model produces wetter soils in lowland areas along stream rills and channels through re-infiltration of lateral overland flow. This water subsidy provides plants with favourable conditions to produce more leaves,  $\text{CO}_2$ , and ET fluxes in lowland areas. This is also consistent with a study conducted by Thompson *et al.* (2011). Thus, overland flow generated by the infiltration-excess mechanism can be regarded as an additional driver for plant growth, and re-infiltration of overland flow over complex terrain may play a role in buffering climatic impacts in semi-arid catchments.

Although the coupled 3D ecohydrological model simulates quite well the integral behaviour of the catchment, e.g. surface water and  $\text{CO}_2$  fluxes averaged over the entire catchment, the modelled soil moisture at 15 cm depth is systematically lower than observations. Accurate modelling of 3D soil moisture distribution is challenging because of the lack of measurements of the distributed features of subsurface soil textures and geophysical properties. Recent developments in advanced techniques to measure 3D distributions of soil properties and soil moisture using electrical and magnetic geophysical sensors and techniques (e.g. Robinson *et al.*, 2008) can help assess and improve advanced 3D modelling of subsurface hydrology at catchment scales. Other

developments that are expected to enhance the current generation of coupled ecohydrological models include representations of processes such as macropore and preferential flow, modules for particle tracking needed for hydrograph separation, and utilities for sensitivity analysis to better deal with uncertain parameterizations and lack of observation data. The coupled model provides a research tool to explore the interactions between hydrological and ecological processes, for instance under climate change or, more specifically in this study, in the context of plant growth in a water-limited grassland catchment.

#### ACKNOWLEDGEMENTS

This work was mainly supported by Biosphere 2 and partly by DOE (DE-SC0006773) and NSF (EF 1065790). Hydrologic, watershed characterization, and flux data were provided by the USDA-ARS, Southwest Watershed Research Center (SWRC), Tucson, AZ. LIDAR data were provided by the SWRC and the University of Florida with funding assistance from the EPA and the US Department of Defense Legacy Program. We commend and gratefully acknowledge the dedication of the ARS Southwest Watershed Research Center for maintaining the Walnut Gulch Experimental Watershed and for their diligent long-term collection of high-quality hydrologic and watershed data. We also wish to thank the two anonymous reviewers for their very helpful comments on the paper.

#### REFERENCES

- Allison SD, Wallenstein MD, Bradford MA. 2010. Soil-carbon response to warming dependent on microbial physiology. *Nature Geoscience*. DOI: 10.1038/NGEO846.
- Barron-Gafford GA, Scott RL, Jenerette GD, Huxman TE. 2011. The relative controls of temperature, soil moisture, and plant functional group on soil CO<sub>2</sub> efflux at diel, seasonal, and annual scales. *Journal of Geophysical Research* **116**: G01023. DOI: 10.1029/2010JG001442.
- Caylor KK, Scanlon TM, Rodriguez-Iturbe I. 2004. Feasible optimality of vegetation patterns in river basins. *Geophysical Research Letters* **31**: L13502. DOI: 10.1029/2004GL020260.
- Charney JG. 1975. Dynamics of deserts and drought in the Sahel. *Quarterly Journal of the Royal Meteorological Society* **101**: 193–202.
- Dickinson RE, Henderson-Sellers A, Kennedy PJ. 1993. Biosphere-Atmosphere Transfer Scheme (BATS) version 1e as coupled to the NCAR Community Climate Model. *NCAR Tech. Note NCAR/TN-3871STR*; 72 pp.
- Emanuel RE, Epstein HE, McGlynn BL, Welsch DL, Muth DJ, D'Odorico P. 2010. Spatial and temporal controls on watershed ecohydrology in the northern Rocky Mountains. *Water Resources Research* **46**: W11553. DOI: 10.1029/2009WR008890.
- Entekhabi D, Eagleson PS. 1989. Land surface hydrology parameterization for atmospheric general circulation models including subgrid-scale spatial variability. *Journal of Climate* **2**: 816–831.
- Famiglietti JS, Wood EF. 1994. Multi-scale modeling of spatially variable water and energy balance processes. *Water Resources Research* **30**(11): 3061–3078.
- Fan Y, Miguez-Macho G, Weaver CP, Walko R, Robock A. 2007. Incorporating water table dynamics in climate modeling: 1. Water table observation and equilibrium water table simulations. *Journal of Geophysical Research* **112**: D10125. DOI: 10.1029/2006JD008111.
- van Genuchten MT, Nielsen DR. 1985. On describing and predicting the hydraulic properties of unsaturated soils. *Annals of Geophysics* **3**(5): 615–628.
- Goodrich DC, Williams DG, Unkrich CL, Hogan JF, Scott RL, Hultine KR, Pool D, Coes AL, Miller A. 2004. Comparison of methods to estimate ephemeral channel recharge, Walnut Gulch, San Pedro River Basin, Arizona. In *Groundwater Recharge in a Desert Environment: The Southwestern United States*, Hogan JF, Phillips FM, Scanlon BR (eds), Water Science and Applications Series, Vol. 9. American Geophysical Union: Washington, DC; 77–99.
- Henderson-Sellers A, Irannejad P, McGuffie K, Pitman AJ. 2003. Predicting land surface climates – better skill or moving targets? *Geophysical Research Letters* **30**(14): 1777. DOI: 10.1029/2003GL017387.
- Idso SB. 1981. A set of equations for full spectrum and 8–14 mm and 10.5–12.5 mm thermal radiation from cloudless skies. *Water Resources Research* **17**: 295–304.
- Jin J, Miller NL. 2007. Analysis of the impact of snow on daily weather variability in mountainous regions. *Journal of Hydrometeorology* **8**: 245–258.
- Kollet SJ. 2009. Influence of soil heterogeneity on evapotranspiration under shallow water table conditions: transient, stochastic simulations. *Environmental Research Letters* **4**: 035007. DOI: 10.1088/1748-9326/4/3/035007
- Kollet SJ, Maxwell RM. 2008. Capturing the influence of groundwater dynamics on land surface processes using an integrated, distributed watershed model. *Water Resources Research* **44**: W02402. DOI: 10.1029/2007WR006004.
- Koster RD, Suarez MJ, Ducharme A, Stieglitz M, Kumar P. 2000. A catchment-based approach to modeling land surface processes in a general circulation model: 1. Model structure. *Journal of Geophysical Research* **105**(D20): 24,809–24,822.
- Liang X, Lettenmaier DP, Wood EF, Burges SJ. 1994. A simple hydrologically based model of land surface water and energy fluxes for general circulation models. *Journal of Geophysical Research* **99**: 14,415–14,428.
- Lu J, Vecchi GA, Reichler T. 2007. Expansion of the Hadley cell under global warming. *Geophysical Research Letters* **34**: L06805. DOI: 10.1029/2006GL028443.
- Maxwell RM, Kollet SJ. 2008. Interdependence of groundwater dynamics and land-energy feedbacks under climate change. *Nature Geoscience* **1**(10): 665–669. DOI: 10.1038/ngeo315.
- Miguez-Macho G, Li HB, Fan Y. 2008. Simulated water table and soil moisture climatology over North America. *Bulletin of the American Meteorological Society* **89**(5): 663–672.
- Moran MS, Emmerich WE, Goodrich DC, Heilman P, Holifield C, Keefer TO, Nearing MA, Nichols MH, Renard KG, Scott RL, Smith JR, Stone JJ, Unkrich CL, Wong JK. 2008. Preface to special section on fifty years of research and data collection: U.S. Department of Agriculture Walnut Gulch Experimental Watershed. *Water Resources Research* **44**: W05S01. DOI: 10.1029/2007WR006083.
- Nash JE, Sutcliffe JV. 1970. River flow forecasting through conceptual models, 1, A discussion of principles. *Journal of Hydrology* **10**: 282–290.
- Niu GY, Paniconi C, Troch PA, Scott RL, Durcik M, Zeng X, Huxman T, Goodrich D. 2013. An integrated modelling framework of catchment-scale ecohydrological processes: 1. Model description and tests over an energy-limited catchment. *Ecohydrology*. DOI: 10.1002/eco.1362.
- Niu GY, Yang ZL, Dickinson RE, Gulden LE. 2005. A simple TOPMODEL-based runoff parameterization (SIMTOP) for use in global climate models. *Journal of Geophysical Research* **110**: D21106. DOI: 10.1029/2005JD006111.
- Niu GY, Yang ZL, Mitchell KE, Chen F, Ek MB, Barlage M, Longuevergne L, Kumar A, Manning K, Niyogi D, Rosero E, Tewari M, Xia YL. 2011. The community Noah land surface model with multiparameterization options (Noah-MP): 1. Model description and evaluation with local-scale measurements. *Journal of Geophysical Research* **116**: D12109. DOI: 10.1029/2010JD015139.
- Pan L, Jin J, Miller N, Wu YS, Bodvarsson G. 2008. Modeling hydraulic responses to meteorological forcing: from canopy to aquifer. *Vadose Zone Journal* **7**: 325–331. DOI: 10.2136/vzj2006.0106.

- Reynolds JF, Smith DMS, Lambin EF, Turner II BL, Mortimore M, Batterbury SPJ, Downing TE, Dowlatabadi H, Fernández RL, Herrick JE, Huber-Sannwald E, Jiang H, Leemans R, T. Lynam, Maestre FT, Ayarza M, Walker B. 2007. Global desertification: building a science for dryland development. *Science* **316**: 847–851.
- Riveros-Iregui DA, Emanuel RE, Muth DJ, McGlynn BL, Epstein HE, Welsch DL, Pacific VJ, Wraith JM. 2007. Diurnal hysteresis between soil CO<sub>2</sub> and soil temperature is controlled by soil water content. *Geophysical Research Letters* **34**: L17404. DOI: 10.1029/2007GL030938.
- Robinson DA, Binley A, Crook N, Day-Lewis FD, Ferre TPA, Grauch VJS, Knoght R, Knoll M, Lakshmi V, Miller R, Nyquist J, Pellerin L, Singha K, Slater L. 2008. Advancing process-based watershed hydrological research using near-surface geophysics: a vision for, and review of, electrical and magnetic geophysical methods. *Hydrological Processes* **22**: 3604–3635.
- Schaefer K, Schwalm CR, Williams C, Arain MA, Barr A, Chen JM, Davis KJ, Dimitrov D, Hilton TW, Hollinger DY, Humphreys E, Poulter B, Raczka BM, Richardson AD, Sahoo A, Thornton P, Vargas R, Verbeeck H, Anderson R, Baker I, Black TA, Bolstad P, Chen J, Curtis PS, Desai AR, Dietze M, Dragoni D, Gough C, Grant RF, Gu L, Jain A, Kucharik C, Law C, Liu S, Lokipitiya E, Margolis HA, Matamala R, McCaughey JH, Monson R, Munger JW, Oechel W, Peng C, Price DT, Ricciuto D, Riley WJ, Roulet N, Tian H, Tonitto C, Torn M, Weng E, Zhou X. 2012. A model-data comparison of gross primary productivity: Results from the North American Carbon Program site synthesis. *Journal of Geophysical Research* **117**: G03010. DOI: 10.1029/2012JG001960.
- Schwalm CR, Williams CA, Schaefer K, Anderson R, Arain MA, Baker I, Barr A, Black TA, Chen G, Chen JM, Ciais P, Davis KJ, Desai A, Dietze M, Dragoni D, Fischer ML, Flanagan LB, Grant R, Gu L, Hollinger D, Izaurrealde RC, Kucharik C, Lafleur P, Law BE, Li L, Li Z, Liu S, Lokupitiya E, Luo Y, Ma S, Margolis H, Matamala R, McCaughey H, Monson RK, Oechel WC, Peng C, Poulter B, Price DT, Ricciuto DM, Riley W, Sahoo AK, Sprintsin M, Sun J, Tian H, Tonitto C, Verbeeck H, Verma SB. 2010. A model-data intercomparison of CO<sub>2</sub> exchange across North America: Results from the North American Carbon Program site synthesis. *Journal of Geophysical Research* **115**: G00H05. DOI: 10.1029/2009JG001229.
- Scott RL, Hamerlynck EP, Jenerette GD, Moran MS, Barron-Gafford GA. 2010. Carbon dioxide exchange in a semidesert grassland through drought-induced vegetation change. *Journal of Geophysical Research* **115**: G03026. DOI: 10.1029/2010JG001348.
- Seager R, Ting M, Held IM, Kushnir Y, Lu J, Vecchi G, Huang H, Harnik N, Leetmaa A, Lau A, Li C, Vélez J, Naik N. 2007. Model projections of an imminent transition to a more arid climate in southwestern North America. *Science* **216**: 1181–1184.
- Sellers PJ, Mintz Y, Sud YC, Dalcher A. 1986. A simple biosphere model (SIB) for use within general circulation models. *Journal of the Atmospheric Sciences* **43**: 505–531.
- Spangler DP. 1969. A geophysical study of the hydrology of the Walnut Gulch Experimental Watershed, Tombstone, Arizona. PhD Dissertation, Dept. of Geology, Univ. of Arizona, Tucson; 103.
- Thompson SE, Harman CJ, Troch PA, Brooks PD, Sivapalan M. 2011. Spatial scale dependence of ecohydrologically mediated water balance partitioning: a synthesis framework for catchment ecohydrology. *Water Resources Research* **47**: W00J03. DOI: 10.1029/2010WR009998.
- Todd-Brown KE, Hopkins FM, Kivlin SN, Talbot JM, Allison SD. 2012. A framework for representing microbial decomposition in coupled climate models. *Biogeochemistry* **09**: 19–33. DOI 10.1007/s10533-011-9635-6.
- Troch PA, Martinez GF, Pauwels VRN, Durcik M, Sivapalan M, Harman C, Brooks PD, Gupta H, Huxman TE. 2009. Climate and vegetation water use efficiency at catchment scales. *Hydrological Processes* **23**: 2409–2414.
- Xue Y, Shukla J. 1993. The influence of land surface properties on Sahel climate. Part I: desertification. *Journal of Climate* **6**: 2232–2245.
- Zeng N, Yoon J. 2009. Expansion of the world's deserts due to vegetation-albedo feedback under global warming. *Geophysical Research Letters* **36**: L17401. DOI: 10.1029/2009GL039699.
- Zeng N, Neelin JD, Lau KM, Tucker CJ. 1999. Enhancement of interdecadal climate variability in the Sahel by vegetation interaction. *Science* **286**: 1537–1540.